Electronic Supplementary Material (ESI) for Inorganic Chemistry Frontiers.

Supporting Information

Solvated/desolvated homochiral Fe(II) complexes showing distinct bidirectional photo-switching due to a hidden state

Xin-Hua Zhao,[a] Yi-Fei Deng,[a] Jia-Quan Huang,[a] Min Liu,[b] and Yuan-Zhu Zhang*[a]

[a] *Department of Chemistry, Southern University of Science and Technology, Shenzhen, 518055, P. R. China.*

[b] *College of Nuclear Science and Technology, University of South China, Hengyang, 421001, P. R. China.*

Physical measurements

Powder X-ray diffraction (PXRD) patterns were recorded on a Rigaku Smartlab X-ray diffractometer. Elemental analyses for C, H, and N were performed on an Elementar Vario EL Cube elemental analyzer. Thermogravimetric analyses (TGA) were carried out under an argon atmosphere at 10 K/min using a METTLER-TOLEDO TG2 instrument. UV-vis spectra in acetonitrile solution at a concentration of 10^{-4} mol L^{-1} were recorded on a Varian Cary 50 spectrophotometer. Circular dichroism (CD) spectra in acetonitrile solution at 10^{-4} mol L^{-1} were recorded on a Chirascan circular dichroism spectrophotometer. ^{57}Fe Mössbauer spectra were recorded on a SEE Co W304 Mössbauer spectrometer using a 57Co/Rh source in transmission geometry, and a temperature controller of helium cryostat (Advanced Research Systems, Inc., 4 K) was used to control temperature. The data were fitted by using the MossWinn 4.0 software. Magnetic measurements were performed on a Quantum Design SQUID MPMS3 magnetometer on the ground single crystals of all complexes. Diamagnetic corrections were calculated from Pascal constants and applied to all the constituent atoms and sample holders.[1] For the photomagnetic experiments, the irradiation was performed on the ground samples at 10 K, and the light from a diode laser (10 mW, 808 or 532 nm; MDL-III -808 nm-19060627, MDL-III-532 nm-19020320, Changchun New Industries Optoelectronics Technology Co., Ltd. (CNI)) was guided via a flexible optical fiber (5 m length; CNI Fiber) into the SQUID magnetometer.

Single crystal X-ray diffraction (SCXRD)

SCXRD data for all the complexes were collected on a Bruker D8 VENTURE diffractometer with graphite monochromated Mo Kα radiation (λ = 0.71073 Å) and at 100 and/or 200 K. Lorentz/polarization corrections were applied during data reduction and the structures were solved by the direct method (SHELXL-2014).[2] Refinements were performed by full-matrix least squares (SHELXL-2014) on F^2 and empirical absorption corrections (SADABS) were applied.[3,4] Anisotropic thermal parameters were used for the non-hydrogen atoms. Hydrogen atoms were added geometrically

and refined using a riding model. Weighted R factors (*wR*) and all the goodness-of-fit (*S*) values are based on F^2; conventional *R* factors (*R*) are based on F, with F set to zero for negative F^2. CCDC: 2299877-2299886 contains the crystallographic data that can be obtained via www.ccdc.cam.ac.uk/conts/retrieving.html (or from the Cambridge Crystallographic Data Centre, 12, Union Road, Cambridge CB21EZ, UK; fax: (+44) 1223-336-033; or deposit@ccdc.cam.ac.uk). The data collection and structure refinement parameters are given in Tables S1–S3 in the Supporting Information, and the selected bond lengths, bond angles, and short contacts are given in Tables S4–S7.

Experimental procedures

The ligands (*S*)-N^1,N^2-dibenzyl-N^1,N^2-bis(pyridin-2-ylmethyl)propane-1,2-diamine (*S*-L) and (*R*)-N^1,N^2-dibenzyl-N^1,N^2-bis(pyridin-2-ylmethyl)propane-1,2-diamine (*R*-L) were prepared by a modified literature method.[5,6]

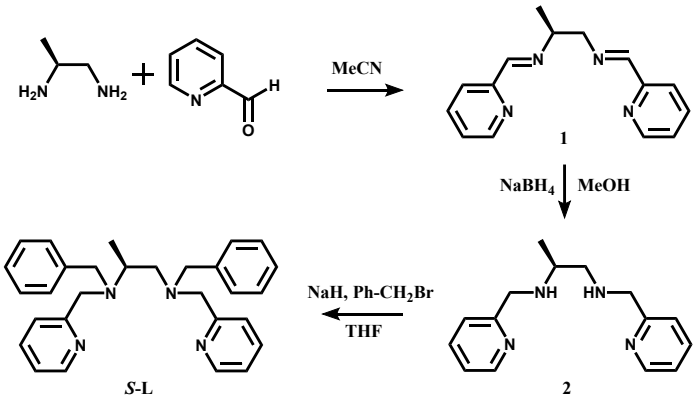

Scheme 1. The synthesis of ligand *S*-L.

S-Propylene 1,2-diamine dihydrochloride (2.94 g, 20 mmol) was suspended in 150 mL of acetonitrile (MeCN). Triethylamine (7.0 mL, 50. mmol) was then added, and the mixture was stirred for 30 minutes at room temperature. Subsequently, pyridine-2-carboxaldehyde (4.28 g, 40. mmol) was added, and the reaction was allowed to stir for approximately 15 hours at room temperature. The mixture was then quenched with H_2O (90 mL), and the aqueous layer was extracted with CH_2Cl_2 (3 × 50 mL). The combined CH_2Cl_2 solution was dried over Na_2SO_4, filtered, and concentrated in vacuo to give the crude Schiff base product of (1*E*,1'*E*)-*N*,*N*'-((*S*)-propane-1,2-diyl)bis(1-(pyridin-2-yl)methanimine) (**1**) as an orange oil. Next, the diimine of **1** (4.30 g, 17 mmol) was dissolved in MeOH (50 mL) with the addition of $NaBH_4$ (1.28 g, 34 mmol)

in portions, and the reaction was stirred for 3 hours at room temperature. After this time, the mixture was quenched with H_2O (30 mL) and acidified with aqueous HCl (2.0 M) until a *p*H < 2 was reached. Aqueous NaOH (2.5 M) was then added until the solution reached a *p*H > 10. The product was extracted with CH_2Cl_2 (3 × 50 mL) and then dried over Na_2SO_4. The solvent was removed under reduced pressure to yield (*S*)-N^1,N^2-bis(pyridin-2-ylmethyl)propane-1,2-diamine (**2**) as a yellow oil: 6.0 g, 83%.

(*S*)-N^1,N^2-bis(pyridin-2-ylmethyl)propane-1,2-diamine (**2**, 3.85 g, 15 mmol) was dissolved in THF (40 mL), and then added dropwise to a suspension of NaH (60% in mineral oil, 1.80 g, 45 mmol) in THF (20 mL). The resulting mixture was stirred for 20 minutes, followed by the addition of benzyl bromide (5.3 mL, 45 mmol). The mixture was then stirred for 16 hours at room temperature. After acidifying (pH < 2) with 2M HCl, the mixture was washed with Et_2O (50 ml). The aqueous layer was treated with 2.5M NaOH until a pH of 14 was reached, and the solution was extracted with CH_2Cl_2 (3 x 50 mL). The combined organic solution was dried with Na_2SO_4 and the solvent was removed under reduced pressure. The crude product was purified by recrystallization with MeOH/CH_2Cl_2 to yield the pure product of (*S*)-N^1,N^2-dibenzyl-N^1,N^2-bis(pyridin-2-ylmethyl)propane-1,2-diamine (*S*-L) as a yellow solid.

For ***S*-L**, Yield: 3.50 g, 53%. ^{1}H NMR ($CDCl_3$, 400 MHz): δ 8.47 (d, J = 5.1 Hz, 1H), 8.44 (d, J = 4.8 Hz, 1H), 7.58 (m, 2H), 7.45 (d, J = 8.1 Hz, 2H), 7.35 (d, J = 7.8 Hz, 2H), 7.30-7.07 (m, 10H), 3.60 (m, 8H), 3.05 (m, 4H), 2.73 (dd, J = 5.3Hz, 7.5 Hz, 1H), 2.43 (dd, J = 8.2 Hz, 4.4 Hz, 1H), 1.08 (d, J = 6.6 Hz, 3H) ppm.

For ***R*-L**, Yield: 3.80 g, 58%. ^{1}H NMR ($CDCl_3$, 400 MHz): δ 8.49 (d, J = 5.0 Hz, 1H), 8.46 (d, J = 4.9 Hz, 1H), 7.60 (m, 2H), 7.48 (d, J = 7.8 Hz, 2H), 7.36 (d, J = 7.4 Hz, 2H), 7.31-7.09 (m, 10H), 3.62 (m, 8H), 3.06 (m, 4H), 2.75 (dd, J = 5.2 Hz, 7.6 Hz, 1H), 2.45 (dd, J = 8.2 Hz, 4.4 Hz, 1H), 1.09 (d, J = 6.5 Hz, 3H) ppm.

Reference

1. R. L. Carlin, Magnetochemistry. Springer-Verlag Press: Berlin, Heidelbeg, 1986.
2. G. M. Sheldrick, *SHELXL-2014*, Program for the solution of crystal structures. University of Göttingen, Göttingen, Germany, 2014.
3. G. M. Sheldrick, *SHELXL-2014*, Program for Crystal Structure Refinement. University of Göttingen, Göttingen, Germany, 2014.
4. G. M. Sheldrick, *SADABS*, v.2.01, Bruker/Siemens Area Detector Absorption Correction Program. Bruker AXS: Madison, Wisconism, 1998.
5. C. Ng, M. Sabat and C. L. Fraser, Metal Complexes with Cis α Topology from Stereoselective Quadridentate Ligands with Amine, Pyridine, and Quinoline Donor Groups, *Inorg. Chem.*, 1999, **38**, 5545-5556.
6. S. Lorenz and B. Plietker, Selectivity Trends in Olefin Epoxidations Catalyzed by (NNNN)Manganese (+II) Complexes using Trifluoroethanol as the Solvent, *ChemCatChem*, 2016, **8**, 3203-3206.

Table S1. Crystallographic data and structure refinement parameters for ***S*1** & ***R*1**.

	***S*1**		***R*1**	
formula	$C_{32}H_{42}B_2FeN_6O$		$C_{32}H_{42}B_2FeN_6O$	
Mr. / g mol^{-1}	604.18		604.18	
T / K	100	200	100	200
Crystal system	monoclinic	monoclinic	monoclinic	monoclinic
Space group	$P2_1$	$P2_1$	$P2_1$	$P2_1$
a, Å	9.4663(10)	9.5547(9)	9.4661(11)	9.5467(11)
b, Å	17.1316(15)	17.2760(12)	17.1346(18)	17.2918(17)
c, Å	10.2029(10)	10.3124(8)	10.1788(12)	10.2875(12)
α, deg	90	90	90	90
β, deg	105.115(4)	105.059(3)	105.081(4)	104.979(4)
γ, deg	90	90	90	90
V, Å^3	1597.4(3)	1643.8(2)	1594.1(3)	1640.6(3)
Z	2	2	2	2
D_{cal}/g cm^{-3}	1.256	1.221	1.259	1.223
2θ range / °	5.052-52.834	4.716-49.42	5.052-52.9	5.006-49.674
completeness	99.7%	99.9%	99.5%	98.5%
residual map, e Å^{-3}	0.43/-0.72	0.92/-0.79	0.52/-0.84	0.95/-1.56
GOOF	1.060	1.010	1.034	1.059
Final indices[I>2σ(I)]	R_1 = 0.0454, wR_2 = 0.0941	R_1 = 0.0811, wR_2 = 0.1923	R_1 = 0.0435, wR_2 = 0.1068	R_1 = 0.0795, wR_2 = 0.2011
Flack parameter	0.048(9)	0.06(2)	0.053(8)	0.155(18)

Table S2. Crystallographic data and structure refinement parameters for ***S*1d** and ***R*1d**.

	***S*1d**		***R*1d**	
formula	$C_{32}H_{42}B_2FeN_6O$		$C_{32}H_{42}B_2FeN_6O$	
Mr. / g mol^{-1}	572.14		572.14	
T / K	100	200	100	200
Crystal system	monoclinic	monoclinic	monoclinic	monoclinic
Space group	$P2_1$	$P2_1$	$P2_1$	$P2_1$
a, Å	9.4191(8)	9.516(3)	9.4203(5)	9.5230(4)
b, Å	16.8953(9)	16.950(5)	16.8995(10)	16.9648(9)
c, Å	10.2864(9)	10.300(3)	10.2868(6)	10.3037(5)
α, deg	90	90	90	90
β, deg	105.571(3)	105.712(10)	105.552(2)	105.7050(10)
γ, deg	90	90	90	90
V, Å^3	1576.9(2)	1599.2(9)	1577.68(16)	1602.48(13)
Z	2	2	2	2
D_{cal}/g cm^{-3}	1.205	1.188	1.204	1.186
2θ range / °	5.096-52.886	5.054-52.868	5.094-52.788	5.05-52.942
completeness	99.8	99.8	99.7	99.6
residual map, e Å^{-3}	0.58/-0.39	0.32/-0.36	0.47/-0.32	0.28/-0.33
GOOF	1.031	1.039	1.033	1.006
Final indices[I>2σ(I)]	R_1 =, 0.0360 wR_2 = 0.0864	R_1 =, 0.0390 wR_2 = 0.0861	R_1 =, 0.0339 wR_2 = 0.0740	R_1 =, 0.0359 wR_2 = 0.0818
Flack parameter	-0.003(9)	-0.012(10)	0.000(8)	0.002(9)

Table S3. Crystallographic data and structure refinement parameters for ***S*1-re** and ***R*1-re**.

	***S*1-re**	***R*1-re**
formula	$C_{32}H_{42}B_2FeN_6O$	$C_{32}H_{42}B_2FeN_6O$
Mr. / g mol^{-1}	604.18	604.18
T / K	100	100
Crystal system	monoclinic	monoclinic
Space group	$P2_1$	$P2_1$
a, Å	9.472(2)	9.4804(12)
b, Å	17.103(4)	17.092(2)
c, Å	10.189(2)	10.1676(11)
α, deg	90	90
β, deg	105.219(11)	105.202(3)
γ, deg	90	90
V, Å^3	1592.9(6)	1589.9(3)
Z	2	2
D_{cal}/g cm^{-3}	1.260	1.262
2θ range / °	4.764 to 49.462	4.766 to 49.52
completeness	99.5%	99.8%
residual map, e Å^{-3}	0.49/-0.67	0.56/-0.71
GOOF	1.082	1.081
Final indices[I>2σ(I)]	R_1 = 0.0544 wR_2 = 0.0942	R_1 = 0.0487 wR_2 = 0.1002
Flack parameter	-0.001(12)	0.034(10)

Table S4. Selected bond lengths [Å] and bond angles [°] for ***S*1**, ***R*1**, ***S*1d** and ***R*1d**.

Bond Lengths [Å]

	***S*1**		***R*1**		***S*1d**		***R*1d**	
	100 K	200 K	100 K	200 K	100 K	200 K	100 K	200 K
Fe1-N1	2.092(4)	2.183(8)	2.063(3)	2.163(7)	2.184(3)	2.187(4)	2.186(3)	2.190(3)
Fe1-N2	2.183(3)	2.290(7)	2.159(3)	2.291(6)	2.284(3)	2.287(4)	2.283(3)	2.287(3)
Fe1-N3	2.167(4)	2.260(7)	2.129(3)	2.236(6)	2.260(3)	2.265(3)	2.264(3)	2.269(3)
Fe1-N4	2.098(4)	2.182(8)	2.073(3)	2.189(7)	2.189(3)	2.195(4)	2.193(3)	2.197(3)
Fe1-N5	2.015(4)	2.109(7)	1.995(3)	2.110(7)	2.100(3)	2.099(4)	2.106(3)	2.104(4)
Fe1-N6	2.020(4)	2.104(8)	1.976(3)	2.116(7)	2.118(4)	2.111(5)	2.120(3)	2.118(4)

Bond Angles [°]

	***S*1**		***R*1**		***S*1d**		***R*1d**	
	100 K	200 K	100 K	200 K	100 K	200 K	100 K	200 K
N1-Fe1-N2	79.16(14)	77.3(3)	79.59(12)	76.9(2)	77.09(11)	76.85(13)	77.08(10)	76.94(11)
N1-Fe1-N3	97.37(14)	97.2(3)	97.32(12)	96.8(2)	97.27(11)	97.40(13)	97.33(10)	97.50(12)
N1-Fe1-N4	174.86(16)	171.6(3)	175.60(13)	171.3(3)	171.12(13)	171.02(15)	170.93(11)	171.21(13)
N3-Fe1-N2	82.69(14)	80.2(3)	83.74(12)	80.4(2)	80.48(11)	80.31(13)	80.61(10)	80.38(11)
N4-Fe1-N2	97.45(14)	96.6(3)	97.53(12)	96.5(2)	96.12(11)	96.28(14)	95.99(10)	96.32(11)
N4-Fe1-N3	78.28(13)	75.8(2)	78.99(12)	76.4(2)	75.74(10)	75.53(12)	75.55(10)	75.60(11)
N5-Fe1-N1	92.45(14)	93.8(3)	91.73(13)	93.6(3)	94.69(12)	94.42(14)	94.89(11)	94.50(13)
N5-Fe1-N2	91.94(16)	92.2(3)	91.56(13)	92.0(3)	91.97(13)	92.17(16)	92.00(12)	92.21(14)
N5-Fe1-N3	167.69(14)	164.8(3)	168.86(12)	165.4(2)	164.03(12)	164.14(14)	163.90(10)	164.06(12)
N5-Fe1-N4	91.53(14)	92.2(3)	91.68(13)	92.2(3)	91.24(12)	91.59(14)	91.16(11)	91.36(13)
N5-Fe1-N6	97.09(16)	99.0(3)	96.54(13)	99.2(2)	100.59(14)	100.53(17)	100.68(12)	100.41(14)
N6-Fe1-N1	91.10(15)	91.3(3)	91.27(13)	91.6(3)	91.02(12)	91.23(15)	90.94(11)	91.18(13)
N6-Fe1-N2	167.02(14)	164.5(2)	167.98(12)	164.4(2)	163.42(11)	163.26(13)	163.30(10)	163.35(12)
N6-Fe1-N3	90.15(14)	91.0(3)	89.77(12)	90.8(2)	89.76(12)	89.78(15)	89.58(11)	89.82(13)
N6-Fe1-N4	91.63(14)	93.6(3)	91.11(12)	93.9(3)	94.40(12)	94.23(16)	94.58(11)	94.21(13)
C30-N5-Fe1	172.9(4)	172.9(9)	172.3(3)	173.0(7)	175.2(3)	173.7(4)	175.4(3)	173.9(3)
C31-N6-Fe1	160.3(4)	157.2(7)	162.3(3)	157.0(6)	158.1(3)	159.8(4)	158.1(3)	159.6(3)

Table S5. Selected short contacts [Å] for ***S*1** and ***R*1**.

	***S*1**		***R*1**		**Symm. op. 2**
	100 K	200 K	100 K	200 K	
C19-H19···π (C30≡N5)	2.7720(2)	2.8056(2)	2.7803(3)	2.8255(3)	-1+x, y, z
C3-H3···B2	2.8709(3)	2.9322(2)	2.8708(3)	2.9179(3)	x, y, -1+z
C19···H13-C13	2.8400(2)	2.8983(2)	2.8345(2)	2.8825(2)	x, y, -1+z
C20···H13-C13	2.8240(2)	2.8903(2)	2.8164(2)	2.8956(2)	x, y, -1+z
C4···B1	3.7304(3)	3.6951(2)		3.6826(3)	1-x, -1/2+y, 1-z
B1···H29-C29	3.1396(3)		3.1181(3)	3.1978(3)	1-x, -1/2+y, 1-z
B1···H7-C7	3.0300(2)	3.0767(2)	3.0337(2)	3.0506(2)	1-x, -1/2+y, 1-z
C9-H9B···H1A-B1	2.3947(2)	2.3106(1)			1-x, -1/2+y, 1-z
C9-H9B···H1C-B1			2.3671(2)	2.5108(2)	1-x, -1/2+y, 1-z
C2-H2···O1	2.5029(2)	2.5607(1)	2.5258(2)	2.6010(2)	x, y, z
C10-H10A···O1	2.6148(2)	2.6589(2)			-1+x, y, -1+z
C10-H10B···O1			2.6140(2)	2.6623(2)	-1+x, y, -1+z
C12-H12···O1	2.4774(2)	2.5343(2)	2.4745(2)	2.5797(2)	-1+x, y, -1+z

Table S6. Selected short contacts [Å] for ***S*1d** and ***R*1d**.

	***S*1d**		***R*1d**		**Symm. op. 2**
	100 K	200 K	100 K	200 K	
C19-H19···π (C30≡N5)	2.6878(2)	2.7198(7)	2.6852(1)	2.7194(1)	1+x, y, z
C3-H3···B2	2.8953(3)	2.9168(1)	2.8874(2)	2.9239(1)	x, y, -1+z
C21···H14-C14	2.8291(2)	2.8422(9)	2.8245(2)	2.8429(1)	x, y, -1+z
C19···H13-C13	2.8925(2)	2.9406(7)	2.8984(1)	2.9443(1)	x, y, -1+z
C20···H13-C13	2.8782(1)	2.9237(7)	2.8791(1)	2.9268(1)	x, y, -1+z
B1-H1B···H7-C7	2.3714(1)	2.2983(5)	2.4027(1)	2.2760(1)	1-x, -1/2+y, 1-z
C4···B1	3.6879(2)	3.7011(8)	3.7012(1)	3.7108(1)	1-x, -1/2+y, 1-z

Table S7. Structural parameters for ***R*1** and ***R*1d**.

	***R*1**		***R*1d**	
	100 K	200 K	100 K	200 K
$\langle Fe\text{-}N\rangle_{avg}$ [Å]	2.066(3)	2.184(7)	2.192(3)	2.194(4)
Σ [°][a]	56.66	72.80	74.77	74.93
Θ [°][b]	189.38	217.13	228.79	230.27
CShM[c]	0.780	1.125	1.239	1.242

[a] Σ for the sum of the deviations from 90° of the 12 cis-angles, [b] Θ for the sum of the deviations from 60° of the 24 trigonal angles of the projection of the [FeN_6] octahedron onto its trigonal faces, [c] *CShM* for the continuous shape measurement relative to the ideal octahedron.

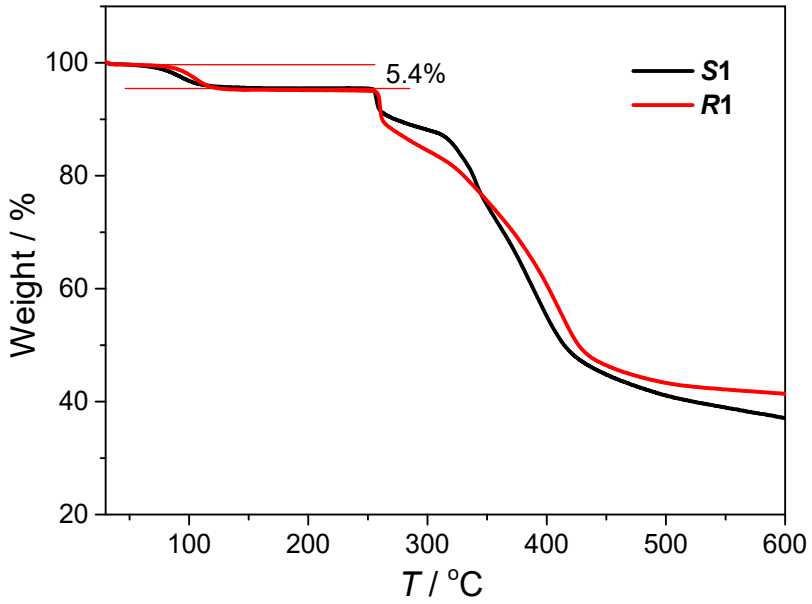

Fig. S1 TGA curves of complexes ***S*1** and ***R*1** at a rate of 10 K/min under an argon atmosphere. The one-step weight loss of 5.4% at around 100 °C agrees well with the losing of one methanol molecule.

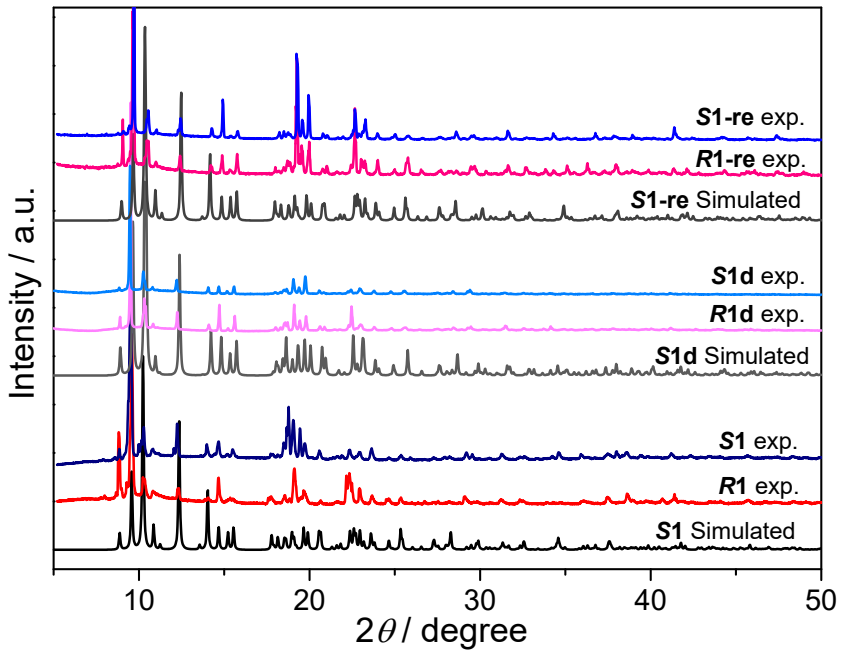

Fig. S2 Experimental and simulated PXRD patterns of ***S*1**, ***R*1**, ***S*1d**, ***R*1d**, ***S*1-re** and ***R*1-re**. The diffraction patterns of all complexes are in good agreement with the simulated one, suggesting their good phase purity.

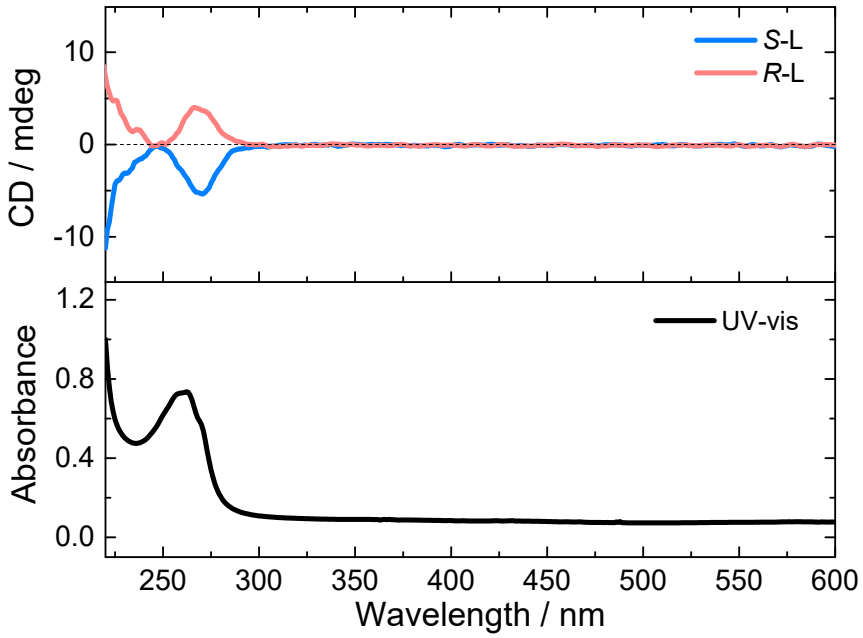

Fig. S3 UV-vis and CD spectra of *S*-L and *R*-L measured in acetonitrile solution.

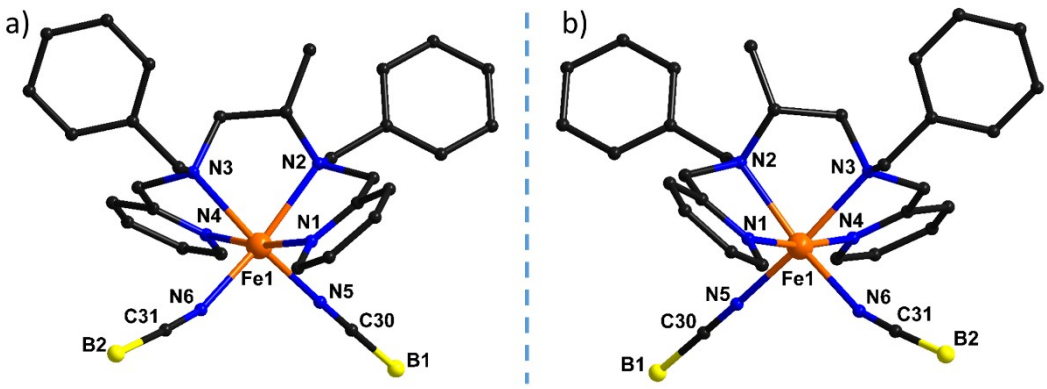

Fig. S4 Crystal structures of a) ***S*1d** and b) ***R*1d** at 200 K. Hydrogen atoms are omitted for clarity.

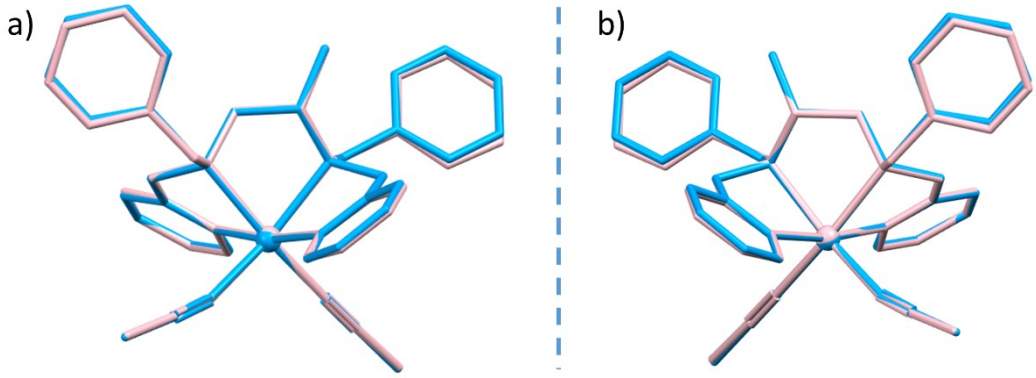

Fig. S5 Minimized overlay of molecular structures for a) ***S*1 / *S*1d** and b) ***R*1 / *R*1d** at 200 K.

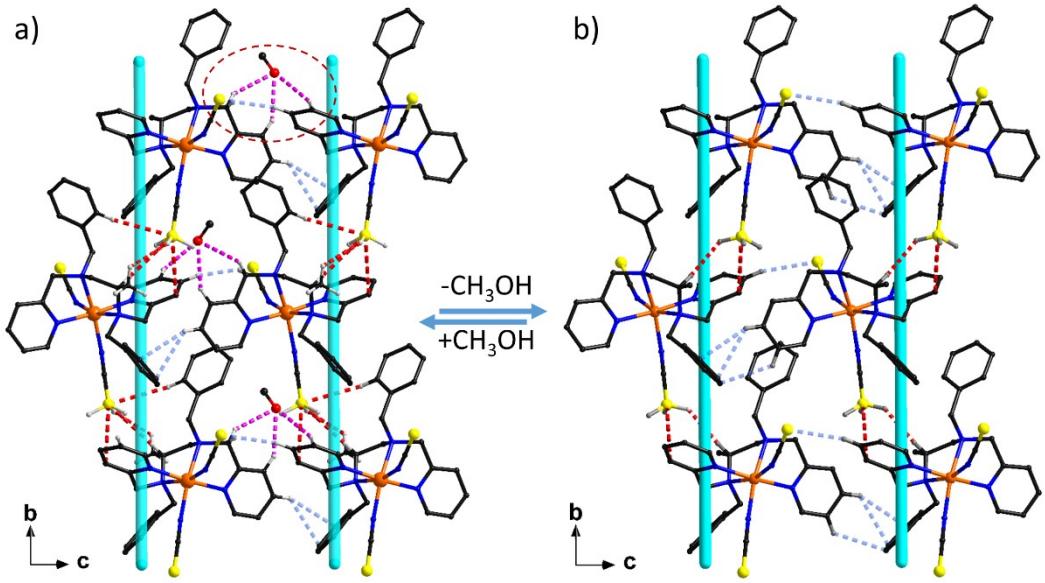

Fig. S6 Spiral diagrams of a) ***R*1** and b) ***R*1d** in the *bc* plane at 200 K. Red dotted lines represent short contacts between BH_3CN^- and ligand *S*-L/*R*-L along the helical chains, light blue dotted lines represent short contacts between neighboring chains, pink dotted lines represent short contacts between MeOH and ligand *S*-L.

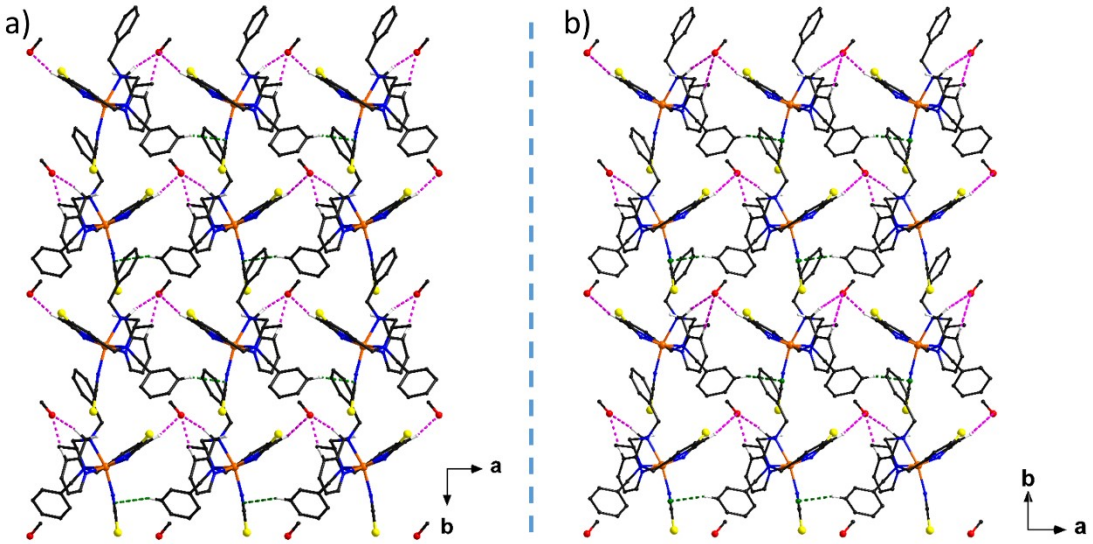

Fig. S7 Crystal packing of a) ***S*1** and b) ***R*1** in the *ab* plane at 200 K. Pink dotted lines represent short contacts between CH_3OH and ligand *S*-L/*R*-L, green dotted lines represent short contacts between $NCBH_3^-$ and benzyl group.

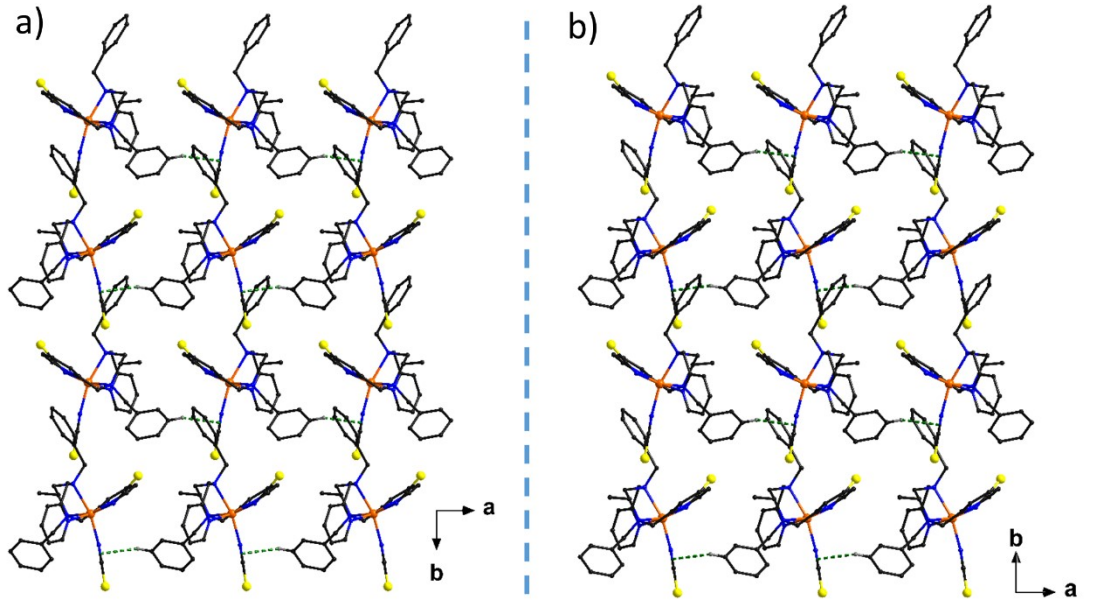

Fig. S8 Crystal packing of a) ***S*1d** and b) ***R*1d** in the *ab* plane at 200 K. Green dotted lines represent short contacts between $NCBH_3^-$ and benzyl group.

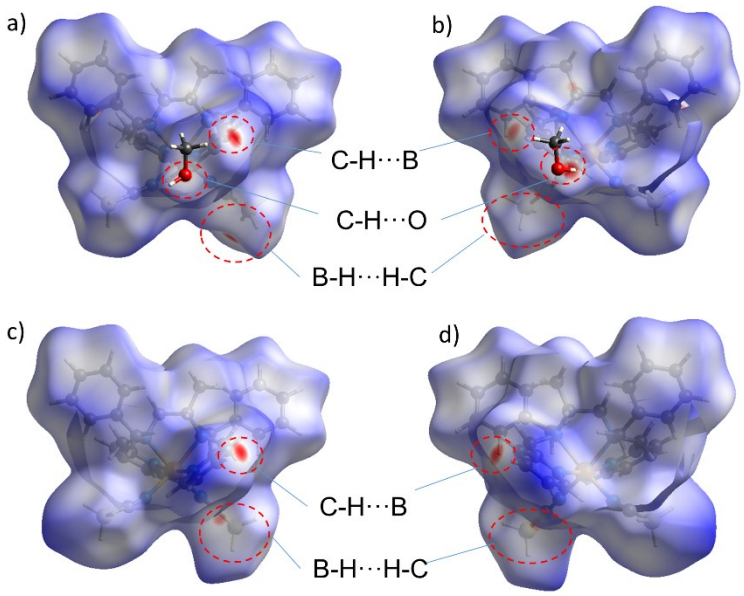

Fig. S9 Hirshfeld surface of [(*S*-L)Fe(NCBH$_3$)$_2$] and [(*R*-L)Fe(NCBH$_3$)$_2$] molecule for complexes a) ***S*1**, b) ***R*1**, c) ***S*1d** and d) ***R*1d** mapped with d_{norm} function, regions of selected interactions are indicated by the red ovals.

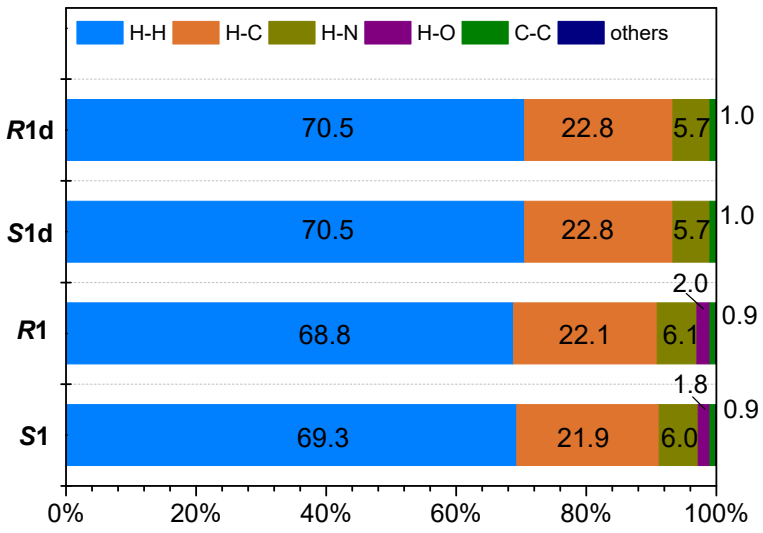

Fig. S10 Percentage contributions of intermolecular interactions for complexes ***S*1**, ***R*1**, ***S*1d** and ***R*1d**.

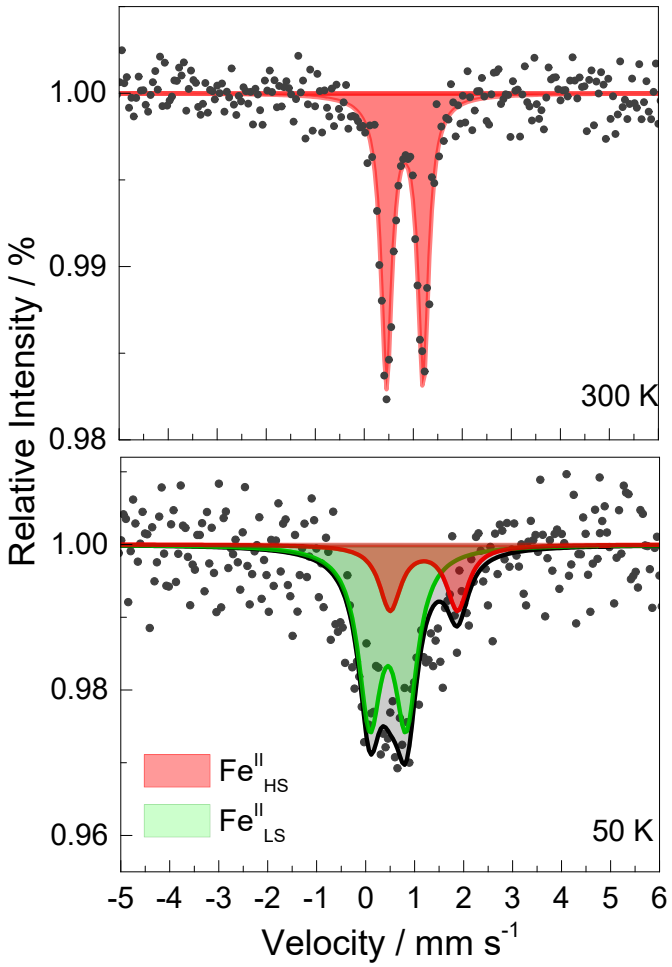

Fig. S11 Mössbauer spectra of ***R*1** at 300 and 50 K.

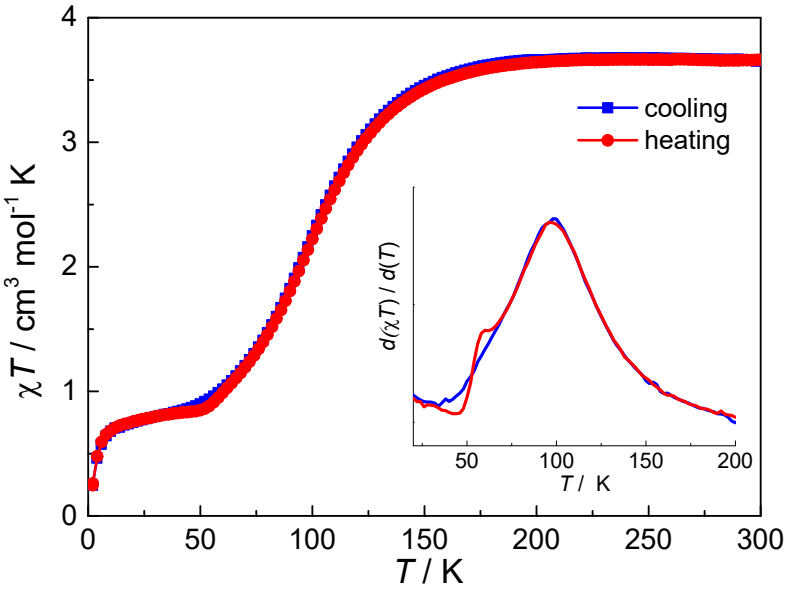

Fig. S12 Temperature-dependent magnetic susceptibilities of ***S*1** in the cooling (blue) and heating (red) modes. Insert: d(χ*T*)/d(*T*) versus *T* plots used to determine $T_{1/2}$.

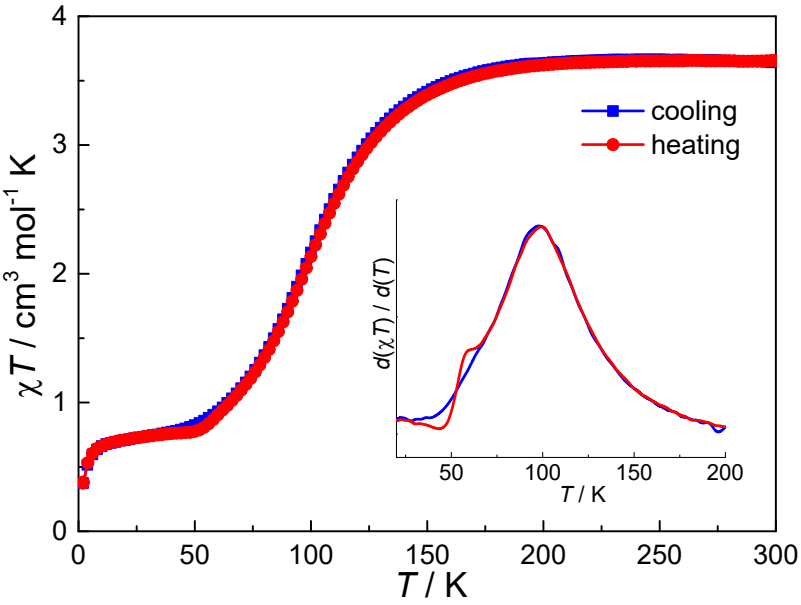

Fig. S13 Temperature-dependent magnetic susceptibilities of ***R*1** in the cooling (blue) and heating (red) modes. Insert: d(χ*T*)/d(*T*) versus *T* plots used to determine $T_{1/2}$.

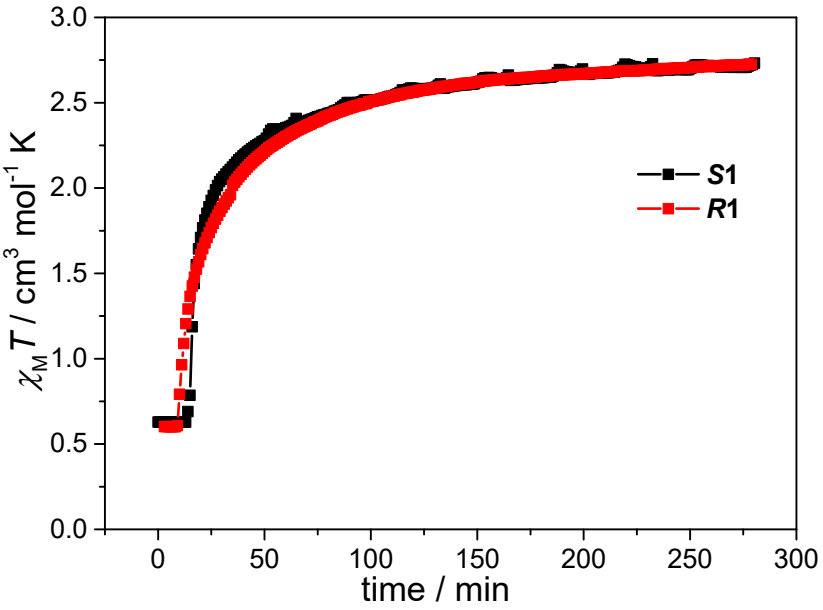

Fig. S14 The χ*T* versus time plots for ***S*1** and ***R*1** irradiated at 532 nm and 10 K.

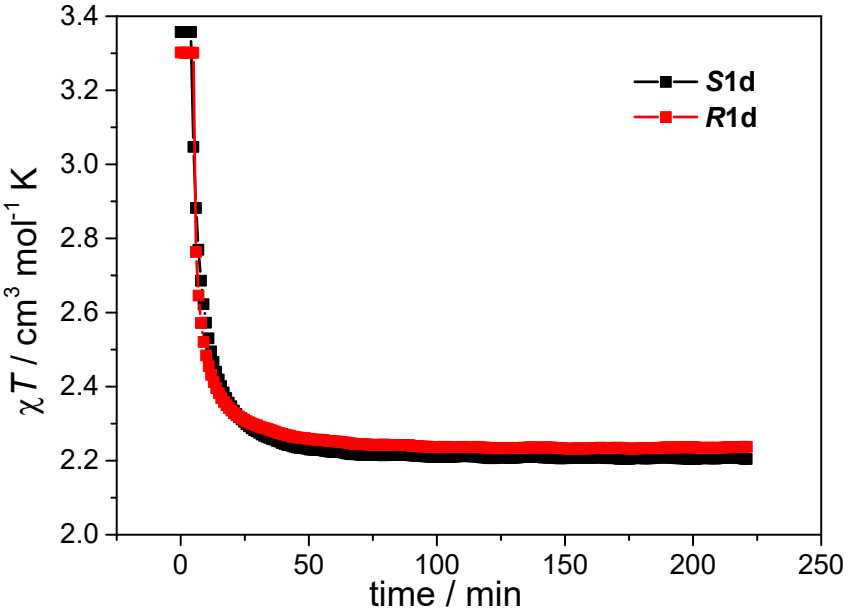

Fig. S15 The χ*T* versus time plots for ***S*1d** and ***R*1d** irradiated at 808 nm and 10 K.

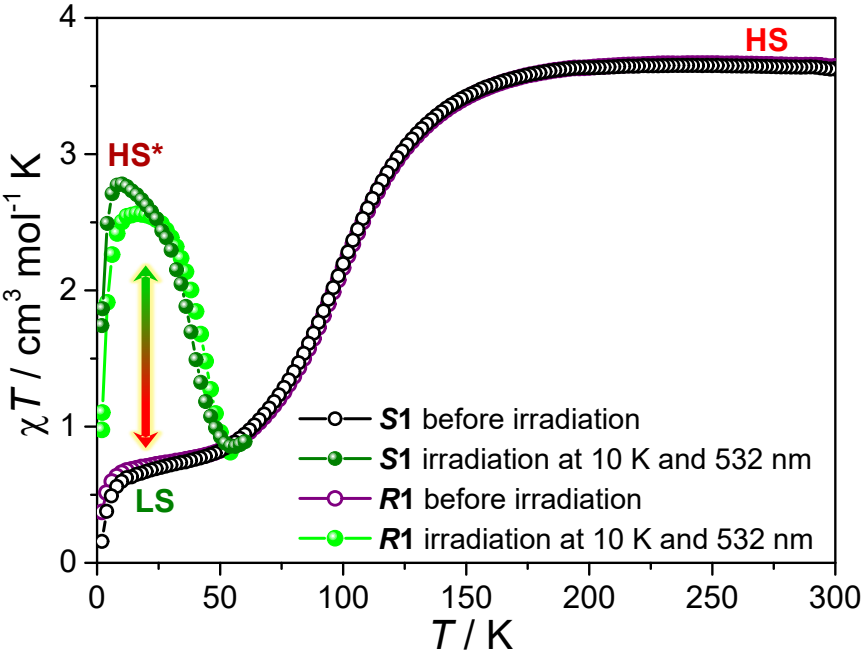

Fig. S16 The χT *vs*. *T* plots for ***S*1** and ***R*1** before and after irradiation.

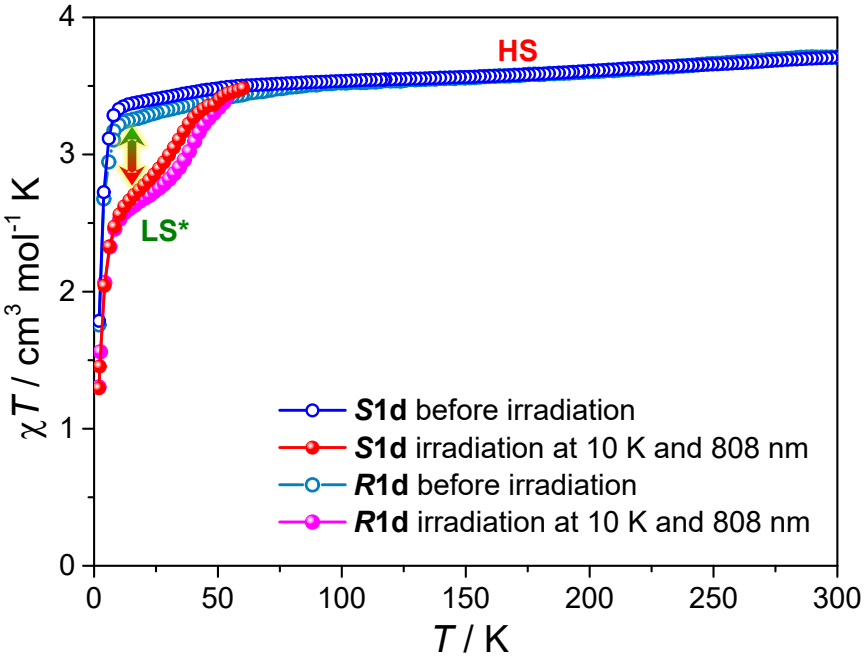

Fig. S17 The χT *vs*. *T* plots for ***S*1d** and ***R*1d** before and after irradiation.

As shown in Fig. S14-S17, the photomagnetic properties of ***R*1** and ***R*1d** are almost identical to those of the *S* enantiomers. We postulate that this similarity is due to the identical coordination environment of the Fe(II) centers and the comparable intermolecular interactions between the *S* and *R* enantiomers.

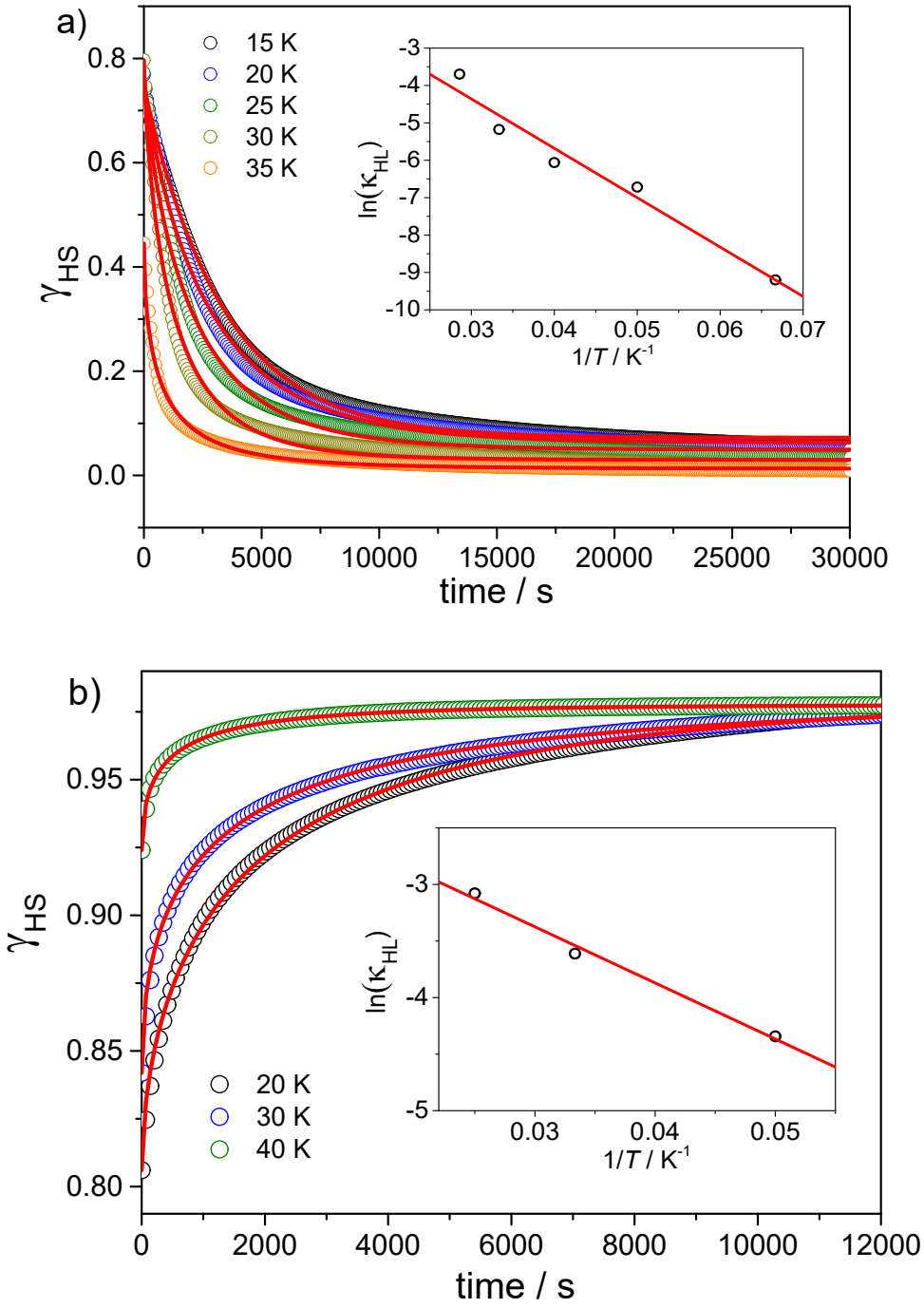

Fig. S18 Relaxation kinetics at various temperatures of the photoinduced HS* or LS* state for a) ***S*1** and b) ***S*1d**. The photoinduced states were reached at 10 K by light irradiation at 532 or 808 nm, the temperature was then increased up to the desired temperature and the light was switched off, the temporal evolution was then recorded at each temperature. The solid lines are for the best fittings based on a stretched exponential behavior. Inset: $\ln(\kappa_{HL})$ versus $1/T$ plot and their linear fit to the Arrhenius equation.

Table S8. The best fitting values for κ_{HL} and κ_{LH} based on a modified stretched exponential law.

T / K	15	20	25	30	35	40
k_{HL} / s^{-1} (***S*1**)	0.000101	0.00121	0.00233	0.00565	0.0248	
κ_{LH} / s^{-1} (***S*1d**)		0.013		0.027		0.046

The relaxation kinetics were analyzed based on a modified stretched exponential law $\gamma_{HS}^{t} = (\gamma_{HS}^{0}-\gamma_{HS}^{R})\exp(-k_{HL}t^{n})+ \gamma_{HS}^{R}$ for ***S*1** and $\gamma_{LS}^{t} = (\gamma_{LS}^{0}-\gamma_{LS}^{R})\exp(-k_{LH}t^{n})+ \gamma_{LS}^{R}$ for ***S*1d**, where k_{HL} and k_{LH} are rate constants; γ_{HS}^{t} / γ_{LS}^{t} and γ_{HS}^{0} / γ_{LS}^{0} are the HS or LS molar fractions measured at time t and 0 after irradiation; γ_{HS}^{R} / γ_{LS}^{R} is the remanent HS or LS molar fraction at time $t\rightarrow\infty$. The best fittings were obtained and the k_{HL} constants are given in Table S8. These resulting k_{HL} values suggested that the relaxation kinetics of LS*→HS for ***S*1d** is slightly faster than that of HS*→LS for ***S*1**. Additionally, the obtained k_{HL} constants were applied to the Arrhenius equation $\ln(k_{HL}) = \ln(A) + E_a / RT$, giving small activation energy E_a of 92 and 34 cm^{-1} and pre-exponential factor A of 0.67 and 0.15 s^{-1} for ***S*1** and ***S*1d**, respectively. However, these results are overestimated because the relaxation processes are governed by the coexistence of quantum tunneling and thermal activation mechanisms below 50 K.